This article has been accepted for publication in a future issue of this journal, but has not been fully edited. Content may change prior to final publication. Citation information: DOI 10.1109/TPWRD.2016.2604295, IEEE Transactions on Power Delivery

Dynamic Model, Control and Stability Analysis of MMC in HVDC Transmission Systems

Majid Mehrasa, Edris Pouresmaeil, *Member*, IEEE, Sasan Zabihi, and João P. S. Catalão, *Senior Member, IEEE*

***Abstract*—A control technique is proposed in this paper for control of modular multilevel converters (MMC) in high-voltage direct current (HVDC) transmission systems. Six independent dynamical state variables are considered in the proposed control technique, including two ac currents, three circulating currents, and the dc-link voltage, for effectively attaining the switching state functions of MMCs, as well as for an accurate control of the circulating currents. Several analytical expressions are derived based on the reference values of the state variables for obtaining the MMC switching functions under steady state operating conditions. In addition, dynamic parts of the switching functions are accomplished by direct Lyapunov method (DLM) to guarantee a stable operation of the proposed technique for control of MMCs in HVDC systems. Moreover, the capability curve (CC) of MMC is developed to validate maximum power injection from MMCs into the power grid and/or loads. The impacts of the variations of MMC output and dc-link currents on the stability of dc-link voltage are also evaluated in detail by small-signal analysis.**

***Index Terms*— High-Voltage Direct Current (HVDC) systems, modular multilevel converter (MMC), direct Lyapunov method (DLM), stability analysis.**

I. NOMENCLATURE

Indices

k	a,b,c
i	1,2

Abbreviations

HVDC	High-Voltage Direct-Current
MMC	Modular Multilevel Converter
DLM	Direct Lyapunov Method
VSC	Voltage-Source Converter
MPC	Model Predictive Control
CC	Capability Curve
KVL	Kirchhoff's Voltage Law
KCL	Kirchhoff's Current Law
SMs	Sub-Modules

Variables

i_{ki}	MMC currents
i_{ulki}	Upper and Lower arm currents
i_{cirki}	Circulating currents of MMCs
i_{dci}	dc link currents of MMCs
i_{dqi}	MMC currents in dq frame
$i_{cirdq0i}$	Circulating currents in dq0
i^*_{dqi}	Reference currents of MMC
$i^*_{cirdq0i}$	Reference circulating current
i^*_{dci}	Reference dc link current
Δi_{dqi}	MMC currents variations
Δi_{dci}	dc link currents variations
I_{avdqi}	Average values of MMC currents
v_{ki}	Output voltages of MMC
v_{ulki}	Upper and Lower arm voltages of MMC
$v_{dc,}$	dc link voltage
v_{dqi}	MMC output voltages in dq frame
v^*_{dqi}	Reference MMC output voltages
v^*_{dc}	Reference dc link voltage
v_{tdqi}	Terminal voltages of MMC
Δv_{dc}	dc link voltage variation
Δv_{dci}	MMC effects on dc link voltage
P_i	MMC active power
ΔP_i	MMC active power variation
Q_i	MMC reactive power
ΔQ_i	MMC reactive power variation
$u_{k(1,2)i}$	MMC switching functions
$u^*_{dq0(12)i}$	Reference MMC switching functions
$u_{dq0(1,2)i}$	MMC switching function in dq frame
$\Delta u_{dq0(1,2)i}$	Dynamic of MMC switching function
$(-\psi, -\chi)$	The center of i_{di}-i_{qi} curve
r	The radius of i_{di}-i_{qi} curve
$(-\psi', -\chi')$	The center of P_i-Q_i curve
r'	The radius of P_i-Q_i curve

Parameters

L	MMC inductance
R	MMC resistance
L_{ul}	Upper and lower arm inductance
R_{ul}	Upper and lower arm resistance
L_t	Equivalent inductance of MMC arm
R_t	Equivalent resistance of MMC arm
C_{dc}	The equivalent capacitance of MMCs
R_{dc}	The total switching loss of MMCs
ω	Angular frequency of MMC voltage
$\alpha_{(1-5)i}$	Coefficients of DLM controller

This work was supported by FEDER funds (European Union) through COMPETE, and by Portuguese funds through FCT, under Projects FCOMP-01-0124-FEDER-020282 (Ref. PTDC/EEA-EEL/118519/2010), UID/CEC/50021/2013 and SFRH/BPD/102744/2014. Also, the research leading to these results received funding from the EU Seventh Framework Programme FP7/2007–2013 under grant agreement no. 309048.

Majid Mehrasa is with Young Researchers and Elite Club, Sari Branch, Islamic Azad University, Sari, Iran. E-mail: m.majidmehrasa@gmail.com.

Edris Pouresmaeil and João P. S. Catalão are with INESC TEC and the Faculty of Engineering of the University of Porto, Porto 4200-465, Portugal, also with C-MAST, University of Beira Interior, Covilhã 6201-001, Portugal, and also with INESC-ID, Instituto Superior Técnico, University of Lisbon, Lisbon 1049-001, Portugal. E-mails: edris.pouresmaeil@gmail.com; catalao@ubi.pt.

Sasan Zabihi is with ABB Australia, MicroGrid, Renewable Integration and Distributed Generation CoC, 3406 Export Drive, Berrimah, Northern Territory 0828, Australia. E-mail: sasanzabihi@gmail.com

This article has been accepted for publication in a future issue of this journal, but has not been fully edited. Content may change prior to final publication. Citation information: DOI 10.1109/TPWRD.2016.2604295, IEEE Transactions on Power Delivery

II. Introduction

Distinguished features of MMCs, including decentralized energy storages, modular structure, easy redundant SMs, simple fault identification and clearance promoted the utilization of MMCs in high and medium voltage/power applications [1-2]. Attentions have been attracted to designing proper controllers [3-5], deriving comprehensive general and inner dynamic models [6-9] and presenting effective modulation methods for the new approach [10-12]. The most significant technology concerned to connecting remotely located off-shore wind farms interest the major industrial centers and up-to-dated researchers in using the different kinds of MMC in VSC-HVDC transmission systems [13-16].

Analyzing detailed mathematical models of MMC utilized in HVDC applications offers simultaneous control of active and reactive power and desired dc link voltage in various operating conditions. In [17] an open-loop strategy is designed for controlling the total amount of energy stored inside the MMC. The control technique employs the steady-state solutions of the dynamic equations to make the system globally asymptotically stable [17]. Generic voltage-based and energy-based control structures for MMC inverters are presented in [18] that include voltage balancing between the upper and lower arms. Then, an improved pulse width modulation based control technique is also proposed in the same reference in order to balance the voltage among arm capacitors. The new technique overcomes some major disadvantages corresponding to the applied voltage balancing methods, such as voltage sorting algorithm, extra switching actions, and interference with output voltage. In [19], a digital plug-in repetitive controller is designed to control a carrier-phase-shift pulse-width-modulation (CPS-PWM)-based MMC. The improved circulating current control method with its stability analysis has the merits of simplicity, versatility, and better performance of circulating harmonic current elimination in comparison with the traditional proportional integral controller [19]. Three cost functions based on an MPC are presented in [20] that result in a reduced number of states considered for the ac-side current, circulating current, and capacitor voltage-balancing controls of an MMC. The duty of the first cost function is controlling the ac-side current without considering redundancy. The second one is for the control of the dc-link current ripple, the transient characteristics of the unbalanced voltage condition, and the circulating current. Finally, the last one is designed for reaching the capacitor voltage balancing and reducing the switching frequency of the SM [20]. In addition to the modeling and control schemes analyzed in [21], a switching-cycle state-space model based on the unused switching states of an MMC and the corresponding control method is proposed in [22].

By calculating the average voltage of all SMs in one arm during each control cycle and comparing it with the capacitor voltage of each SM, the switching state of each SM in MMCs is obtained in [23]. In this method, a little sorting of the capacitor voltages is employed and consequently the calculation burden on the controller is significantly decreased.

In order to investigate the impact of the voltage-balancing control on the switching frequency in an MMC, the dynamic relations between the SM's capacitor unbalanced voltage and converter switching frequency are achieved in [24]. Furthermore, by considering negative effects of the unbalanced voltage on the SM capacitor voltage ripple and voltage/current harmonics, the design interaction between switching frequency and SM capacitance, as well as the selection of unbalanced voltage, are also accomplished in [24]. A control technique targeting independent management of capacitor's average voltage in each MMC arm is performed in [25]. In this method, a decomposition of arms energy in different components is considered based on the symmetries of MMC arms. By considering the effects of ac and dc systems, a dynamic MMC model with four independent components of upper and lower arm currents are introduced in [26]. By using this model, dynamical analysis of currents and also design and implementation of current controllers are become simplified.

A dynamic model, control and stability analysis of MMC-HVDC transmission systems is presented in this paper. The main contributions are fourfold:

(1) obtaining a comprehensive dynamic model in d-q frame for MMC-based HVDC system with six independent dynamical state variables, including two ac currents, three circulating currents, and the dc-link voltage.

(2) developing the dynamic parts of switching functions by the use of DLM to reach globally asymptotical stability.

(3) deriving a detailed capability curve (CC) based on active and reactive power of the MMC for the proposed system, investigating the impacts of various values of the dc-link currents on CC; it can be used to verify the maximum capacity of interfaced MMC for injection of active and reactive power into the power grid.

(4) performing a comprehensive investigation of MMC output and dc-link current variations effects on dc-link voltage stability by using small-signal analysis.

The rest of this paper is organized into seven sections. Following the introduction, the dynamic model of MMC-based HVDC is presented in Section III. Steady state analysis of the proposed model is provided in Section IV, while dynamic stability analysis is assessed in Section V. In Section VI, capability curve analysis of MMC is executed, and dc-link voltage stability analysis is performed in Section VII. Simulation results and conclusion are presented in Sections VIII and IX.

III. The Proposed MMC-based HVDC Model

The proposed MMC-based HVDC transmission system with two three-phase transformers utilized for the aims of insulation and voltage conversion are illustrated in Fig. 1.

Each MMC is composed of six SMs in its either upper or lower arms along with relevant resistance and inductance to mimic arm losses and limit arm-current harmonics and fault currents, respectively.

R_{dc} is the total switching loss of MMCs. Considering each SM to be an IGBT half-bridge converter, rudimentary operational manner of SMs can be explicitly seen throughout dynamic analysis of MMC.

Furthermore, the two ac systems are linked to the transformers through resistances and inductances of ac side as shown in Fig. 1.

This article has been accepted for publication in a future issue of this journal, but has not been fully edited. Content may change prior to final publication. Citation information: DOI 10.1109/TPWRD.2016.2604295, IEEE Transactions on Power Delivery

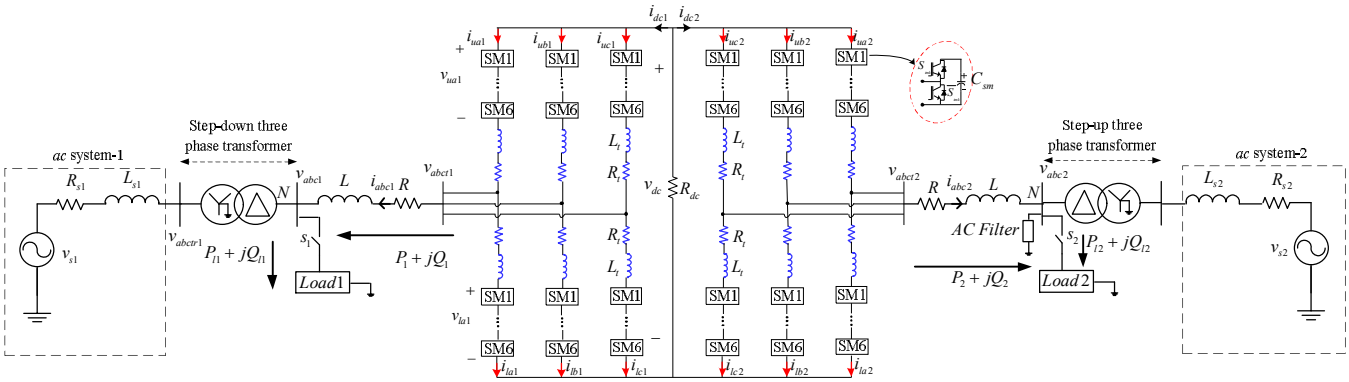

Fig. 1. General model of the proposed MMC-based HVDC system.

A. The mathematical model

As can be seen in Fig. 1, grounding points are considered at each neutral point of ac systems and transformers with Y connection.

Ascertaining another grounding point in the dc-link voltage of MMCs, (1) and (2) are obtained by applying KVL law to the loop including dc-link and MMC ac-side voltages as,

$$v_{ki} + L\frac{di_{ki}}{dt} + Ri_{ki} + L_u\frac{di_{uki}}{dt} + R_u i_{uki} - \frac{v_{dc}}{2} + v_{uki} = 0 \quad (1)$$

$$-v_{ki} - L\frac{di_{ki}}{dt} - Ri_{ki} + L_l\frac{di_{lki}}{dt} + R_l i_{lki} - \frac{v_{dc}}{2} + v_{lki} = 0 \quad (2)$$

Following variables are defined as,

$$i_{ki} = i_{uki} - i_{lki},\ i_{cirki} = \frac{i_{uki} + i_{lki}}{2} - \frac{i_{dci}}{3},\ u_{k1i} = \frac{v_{uki} - v_{lki}}{2},\ u_{k2i} = \frac{v_{uki} + v_{lki}}{2} \quad (3)$$

Subtracting and summing up (1) from and to (2), besides using the defined terms in (3), the dynamic equations of MMCs can be achieved as,

$$\left(\frac{2L + L_t}{2}\right)\frac{di_{ki}}{dt} + \left(\frac{2R + R_t}{2}\right)i_{ki} + u_{k1i} + v_{ki} = 0 \quad (4)$$

$$L_t\frac{di_{cirki}}{dt} + R_t i_{cirki} + R_t\frac{i_{dci}}{3} + u_{k2i} - \frac{v_{dc}}{2} = 0 \quad (5)$$

The equivalent circuits of (4) and (5) are drawn in Fig. 2. The output currents of MMCs can be controlled by accurate analysis of the circuit shown in Fig. 2(a) and thus the switching function of u_{k1i} is a key factor to regulate MMCs active and reactive power acquired by output currents and voltages.

As shown in Fig. 2(b), mitigation of circulating currents is depending on the appropriate adjustment of dc link voltage of MMCs. In addition, the switching function of u_{k2i} plays an important role in effective minimization of undesirable distortions caused by MMC's circulating currents.

The dynamic relations between dc-link voltage and the upper or lower arms currents can be derived by applying a KCL to the dc-link of Fig. 1,

$$C_{dc}\frac{dv_{dc}}{dt} + \frac{v_{dc}}{R_{dc}} + \left(i_{uai} + i_{ubi} + i_{uci}\right) + i_{dci'} = 0 \quad (6)$$

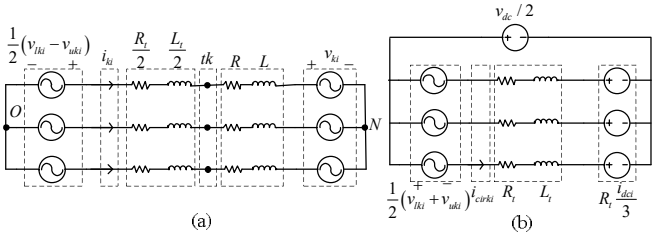

Fig. 2. Equivalent circuits of: (a) Dynamic model based on MMC output currents, (b) dynamic model based on circulating currents.

$$C_{dc}\frac{dv_{dc}}{dt} + \frac{v_{dc}}{R_{dc}} + \left(i_{lai} + i_{lbi} + i_{lci}\right) + i_{dci'} = 0 \quad (7)$$

By adding (6) and (7) and also using the relationship of circulating current in (3), the dynamic relation of dc-link voltage and circulating currents is deduced as,

$$C_{dc}\frac{dv_{dc}}{dt} + \frac{v_{dc}}{R_{dc}} + i_{cirai} + i_{cirbi} + i_{circi} + i_{dc1} + i_{dc2} = 0 \quad (8)$$

By applying Park's transformation to the (4), (5), and (8), general dynamic equations of the proposed model in *0dq* reference frame and based on a selected set of state variables including MMC's output currents, circulating currents and also dc-link voltage can be expressed as,

$$\left(\frac{2L + L_t}{2}\right)\frac{di_{di}}{dt} + \left(\frac{2R + R_t}{2}\right)i_{di} - \omega\left(\frac{2L + L_t}{2}\right)i_{qi} + u_{d1i} + v_{di} = 0$$

$$\left(\frac{2L + L_t}{2}\right)\frac{di_{qi}}{dt} + \left(\frac{2R + R_t}{2}\right)i_{qi} + \omega\left(\frac{2L + L_t}{2}\right)i_{di} + u_{q1i} + v_{qi} = 0$$

$$L_t\frac{di_{cirdi}}{dt} + R_t i_{cirdi} - \omega L_t i_{cirqi} + u_{d2i} = 0 \quad (9)$$

$$L_t\frac{di_{cirqi}}{dt} + R_t i_{cirqi} + \omega L_t i_{cirdi} + u_{q2i} = 0$$

$$L_t\frac{di_{cir0i}}{dt} + R_t i_{cir0i} + u_{02i} - \frac{3\sqrt{2}v_{dc}}{2} + \sqrt{2}R_t i_{dci} = 0$$

$$C_{dc}\frac{dv_{dc}}{dt} + \frac{v_{dc}}{R_{dc}} + \sqrt{3}i_{cir0i} + i_{dc1} + i_{dc2} = 0$$

The needs for reaching well-designed current control loops and guaranteeing desirably balanced operation of dc-link and SM voltages verify that the different parts of (9) should be accurately identified for a fine design of the proposed controller to attain respective aims. The following sections will cover all mentioned points.

This article has been accepted for publication in a future issue of this journal, but has not been fully edited. Content may change prior to final publication. Citation information: DOI 10.1109/TPWRD.2016.2604295, IEEE Transactions on Power Delivery

IV. Steady State Analysis

The state variables of the proposed model should be kept in their desired values in steady state operating condition, regardless of experiencing new circumstances such as a step load change. Consequently, the reference values i_{di}^* and i_{qi}^* are calculated as demonstrated in Fig. 3. As a matter of fact, the q component of ac voltages should be equal to zero for balanced and sinusoidal ac systems. This means that the reference values of MMCs ac voltages are approached to $v_{di} = v_{di}^*$ and $v_{qi}^* = 0$. Based on two first terms of (9) and with respect to the above points, the first switching state functions of MMC in steady state operating condition are derived as shown in Fig.4:

$$u_{d1i}^* = -\left(\frac{2L+L_t}{2}\right)\frac{di_{di}^*}{dt} - \left(\frac{2R+R_t}{2}\right)i_{di}^* + \omega\left(\frac{2L+L_t}{2}\right)i_{qi}^* - v_{di}^*$$
$$u_{q1i}^* = -\left(\frac{2L+L_t}{2}\right)\frac{di_{qi}^*}{dt} - \left(\frac{2R+R_t}{2}\right)i_{qi}^* - \omega\left(\frac{2L+L_t}{2}\right)i_{di}^* \quad (10)$$

In the same condition, the circulating currents of MMCs should be governed to become zero, $i_{cirdi}^* = i_{cirqi}^* = i_{cir0i}^* = 0$. As a result, the second switching functions of MMCs are obtained in accordance to (9) and given in Fig. 5.

$$u_{d2i}^* = 0,\ \ u_{q2i}^* = 0,\ \ u_{02i}^* = \frac{3\sqrt{2}v_{dc}^*}{2} - \sqrt{2}R_t i_{dci}^* \quad (11)$$

Combining (10) and (11) leads to the main upper and lower switching functions of MMCs in steady state operation. Using the last term of (9), the dynamic of dc link voltage in steady state can be expressed as,

$$\frac{dv_{dc}^*}{dt} = -\frac{v_{dc}^*}{C_{dc}R_{dc}} - \frac{i_{dc1}^*}{C_{dc}} - \frac{i_{dc2}^*}{C_{dc}} \quad (12)$$

Equation (12) shows the dynamic relation between dc link voltage and currents of MMCs. Under the steady state operation, dc link voltage will be equal to,

$$v_{dc}^* = -R_{dc}\left(i_{dc1}^* + i_{dc2}^*\right) \quad (13)$$

Equation (13) shows that dc link voltage is dependent on dc currents of MMCs in steady state operating condition. Since dc currents of MMCs are related to the lower and upper MMCs currents, it is understood from (13) that a proper control of output and circulating currents of MMCs yields a balanced value for dc link voltage of MMCs.

V. Dynamic Stability Analysis

An accurate operation of the system can be provided by taking all possible dynamic changes into account. Dynamic presentation of all state variables involved in the proposed HVDC system can be stated as,

$$x_{1i} = i_{di} - i_{di}^*,\ x_{2i} = i_{qi} - i_{qi}^*,\ x_{3i} = i_{cirdi} - i_{cirdi}^*$$
$$x_{4i} = i_{cirqi} - i_{cirqi}^*,\ x_{5i} = i_{cir0i} - i_{cir0i}^*,\ x_{6i} = v_{dc} - v_{dc}^* \quad (14)$$

Total dynamic saved energy is a basic requirement for DLM. Following the points discussed above, the dynamic energy function of the proposed model can be calculated as,

$$H(\bar{x}_i) = \frac{2L+L_t}{4}x_{1i}^2 + \frac{2L+L_t}{4}x_{2i}^2 + \frac{L_t}{2}x_{3i}^2 + \frac{L_t}{2}x_{4i}^2 + \frac{L_t}{2}x_{5i}^2 + \frac{C_{dc}}{2}x_{6i}^2 \quad (15)$$

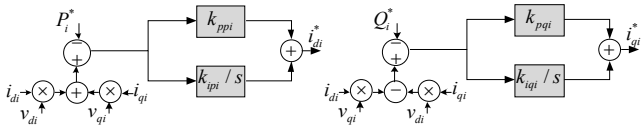

Fig. 3. Calculation of MMC output currents.

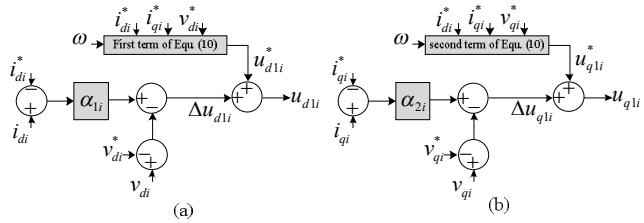

Fig. 4. Switching functions based on MMC output currents (a) d-component, (b) q-component.

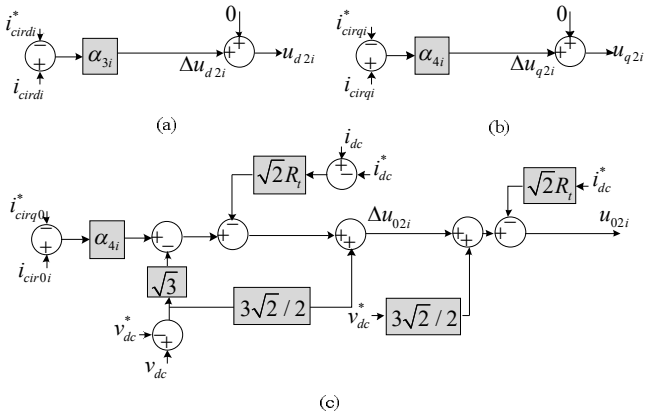

Fig. 5. Switching functions based on circulating currents (a) d-component, (b) q-component, (c) 0-component.

The time-based derivation of (15) can be expressed as,

$$\dot{H}(\bar{x}_i) = \frac{2L+L_t}{2}x_{1i}\dot{x}_{1i} + \frac{2L+L_t}{2}x_{2i}\dot{x}_{2i} + L_t x_{3i}\dot{x}_{3i} + L_t x_{4i}\dot{x}_{4i} + L_t x_{5i}\dot{x}_{5i} + C_{dc}x_{6i}\dot{x}_{6i} \quad (16)$$

Each part of (16) can be obtained from (9) and (14) as,

$$\frac{2L+L_t}{2}\dot{x}_{1i}x_{1i} = -\left(\frac{2R+R_t}{2}\right)x_{1i}^2 + \omega\left(\frac{2L+L_t}{2}\right)\times x_{2i}x_{1i} - \left(u_{d1i} - u_{d1i}^*\right)x_{1i} - \left(v_{di} - v_{di}^*\right)x_{1i}$$
$$\frac{2L+L_t}{2}\dot{x}_{2i}x_{2i} = -\left(\frac{2R+R_t}{2}\right)x_{2i}^2 - \omega\left(\frac{2L+L_t}{2}\right)\times x_{1i}x_{2i} - \left(u_{q1i} - u_{q1i}^*\right)x_{2i} - \left(v_{qi} - v_{qi}^*\right)x_{2i}$$
$$L_t\dot{x}_{3i}x_{3i} = -R_t x_{3i}^2 + \omega L_t x_{4i}x_{3i} - \left(u_{d2i} - u_{d2i}^*\right)x_{3i}$$
$$L_t\dot{x}_{4i}x_{4i} = -R_t x_{4i}^2 - \omega L_t x_{3i}x_{4i} - \left(u_{q2i} - u_{q2i}^*\right)x_{4i}$$
$$L_t\dot{x}_{5i}x_{5i} = -R_t x_{5i}^2 - \left(u_{02i} - u_{02i}^*\right)x_{5i} + \frac{3\sqrt{2}}{2}\left(v_{dc} - v_{dc}^*\right)x_{5i} - \sqrt{2}R_t\left(i_{dci} - i_{dci}^*\right)x_{5i}$$
$$c_{dc}\dot{x}_{6i}x_{6i} = -\frac{x_{6i}^2}{R_{dc}} - \sqrt{3}x_{5i}x_{6i} - \left(i_{dc1} - i_{dc1}^*\right)x_{6i} - \left(i_{dc2} - i_{dc2}^*\right)x_{6i} \quad (17)$$

This article has been accepted for publication in a future issue of this journal, but has not been fully edited. Content may change prior to final publication. Citation information: DOI 10.1109/TPWRD.2016.2604295, IEEE Transactions on Power Delivery

In addition, the MMCs switching functions are extended to (18) with dynamic components which are used by the proposed controller during dynamic changes,

$$u_{dq(12)i} = \Delta u_{dq(12)i} + u^{*}_{dq(12)i} \tag{18}$$

The first part of (18), $\Delta u_{dq(12)i}$, is the dynamic part of the MMC switching functions in d-q reference frame that can be achieved by DLM. This part is responsible to maintain the stability of the proposed model against load variations. Second part of (18) is related to the steady state part of MMC switching functions shown as $u^{*}_{dq(12)i}$. This part is employed so that the state variables of the proposed model follow a special reference values without any dynamic change.

By substitution of (17) and (18) in (16), the summarized derivation of MMCs total saved energy is attained as (19),

$$\begin{aligned}\dot{H}(\bar{x}_i) = &-\left(\frac{2R+R_t}{2}\right)x_{1i}^2 - \left(\frac{2R+R_t}{2}\right)x_{2i}^2 - R_t x_{3i}^2 - R_t x_{4i}^2 - R_t x_{5i}^2 \\ &-\left(\Delta u_{d1i} + \left(v_{di} - v^{*}_{di}\right)\right)x_{1i} - \left(\Delta u_{q1i} + \left(v_{qi} - v^{*}_{qi}\right)\right)x_{2i} - \left(\Delta u_{d2i}\right)x_{3i} \\ &-\left(\Delta u_{q2i}\right)x_{4i} - \left(\Delta u_{02i} - \frac{3\sqrt{2}}{2}x_{6i} + \sqrt{2}R_t\left(i_{dci} - i^{*}_{dci}\right) + \sqrt{3}x_{6i}\right)x_{5i} \\ &-\left(\left(\left(i_{dc1} - i^{*}_{dc1}\right) + \left(i_{dc2} - i^{*}_{dc2}\right)\right)x_{6i} + \frac{x_{6i}^2}{R_{dc}}\right)\end{aligned} \tag{19}$$

According to DLM, a time-varying system with certain state variables will become asymptotically globally stable, if the total saved energy function of system is positive and its derivative is definitely negative.

Therefore, taking into account DLM principle and all terms present in (19), the dynamic components of the MMCs switching functions are,

$$\begin{aligned}&\Delta u_{d1i} = \alpha_{1i}x_{1i} - \left(v_{di} - v^{*}_{di}\right),\ \Delta u_{q1i} = \alpha_{2i}x_{2i} - \left(v_{qi} - v^{*}_{qi}\right) \\ &\Delta u_{d2i} = \alpha_{3i}x_{3i},\quad \Delta u_{q2i} = \alpha_{4i}x_{4i} \\ &\Delta u_{02i} = \alpha_{5i}x_{5i} - \left(-\frac{3\sqrt{2}}{2}x_{6i} + \sqrt{2}R_t\left(i_{dci} - i^{*}_{dci}\right) + \sqrt{3}x_{6i}\right)\end{aligned} \tag{20}$$

The coefficients of α_{3i} are the effective factors for regulating the dynamic parts of the proposed controller that should be chosen appropriately [27]. Terms of (20) guarantee the ultimate designed controller operation against any sudden dynamic changes. As can be seen in (20), due to presence of steady state values in (20), the accurate performance of dynamic parts of switching function are highly reliant on the correct functioning of the proposed model in steady state conditions. Considering (20), all terms available in (19) can evidently identified to be negative values or zero except for the last term that is,

$$-\left(\left(\left(i_{dc1} - i^{*}_{dc1}\right) + \left(i_{dc2} - i^{*}_{dc2}\right)\right)x_{6i} + \frac{x_{6i}^2}{R_{dc}}\right) \tag{21}$$

By assuming balanced MMCs circulating currents, equation (8) can be rewritten as,

$$C_{dc}\frac{dv_{dc}}{dt} + \frac{v_{dc}}{R_{dc}} + i_{dc1} + i_{dc2} = 0 \tag{22}$$

Eq. (21) can also be restated with respect to (14) and (22) as,

$$C_{dc}x_{6i}\frac{dx_{6i}}{dt} \tag{23}$$

In order to investigate the impact of (23) on (19), the various possible amounts that exist for (23) are discussed in this section. Fig. 6 shows the various states of (23). Noticing the reference value demonstrated in red, two possible constant and fluctuated states are considered for dc-link voltage as shown in Fig. 6. The constant states specified with state 1 and state 2 can be more or less than the reference value (for equal value, $x_{6i} = 0$). For fluctuated cases, three states are considered. As can be seen in Fig. 6, for the states of 1 and 2, (23) is equal to zero ($dx_{6i}/dt=0$). Moreover, for fluctuated states, since the sign of dx_{6i}/dt is varying due to the variation of voltage slopes, the ultimate value of (23) becomes periodically positive or negative as depicted in Fig. 6. This is indicating that (23) is always close to zero in other states and consequently not able to noticeably impact the negative value of (19). Therefore, the whole term of (19) is definitely negative or zero.

VI. Capability Curve Analysis of the MMCs

Identifying maximum capability of each MMC in active and reactive power injection during operating condition of HVDC system leads to a more accurate design for the controller. The relation between the dc-link voltage and the ac side voltage of each MMC shown in Fig. 1 can be achieved as,

$$v_{dc}i_{dci} = v_{tdi}i_{di} + v_{tqi}i_{qi} \tag{24}$$

In addition, the relation between the ac side and the output voltage of each MMC in d-q frame can be driven by applying KVL's law to Fig. 1,

$$\begin{aligned}v_{tdi} &= v_{di} + L\frac{di_{di}}{dt} + Ri_{di} - \omega L i_{qi} \\ v_{tqi} &= v_{qi} + L\frac{di_{qi}}{dt} + Ri_{qi} + \omega L i_{di}\end{aligned} \tag{25}$$

By assuming $di_{dqi}/dt=I_{avdqi}$ and substituting (25) in (24), the following circle is obtained as,

$$\begin{aligned}&\left(i_{di} + \psi\right)^2 + \left(i_{qi} + \chi\right)^2 = r^2 \\ &\psi = \frac{LI_{avdi} + v_{di}}{2R},\ \chi = \frac{LI_{avqi} + v_{qi}}{2R} \\ &r = \sqrt{\frac{\left(LI_{avdi} + v_{di}\right)^2 + \left(LI_{avqi} + v_{qi}\right)^2 + 4Rv_{dc}i_{dci}}{4R^2}}\end{aligned} \tag{26}$$

Equation (26) is a circle with the center of $(-\psi, -\chi)$ and radius of r. This circle describes a given area of MMC output current based on a dq frame in which the maximum and minimum values of the current can be accurately calculated.

By substituting $i_{di}=P_i/v_{di}$ and $i_{qi.}=-Q_i/v_{di}$ in (26), the following relation is obtained as,

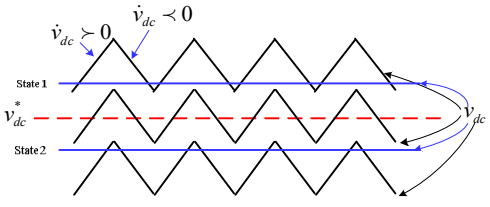

Fig. 6. Different states of v_{dc} and dv_{dc}/dt.

This article has been accepted for publication in a future issue of this journal, but has not been fully edited. Content may change prior to final publication. Citation information: DOI 10.1109/TPWRD.2016.2604295, IEEE Transactions on Power Delivery

$$\left(P_i+\psi'\right)^2+\left(Q_i+\chi'\right)^2=r'^2\Rightarrow\psi'=v_{di}\psi,\ \chi'=-v_{di}\chi,\ r'=v_{di}r \tag{27}$$

The relation described in (27) is the capability curve of MMC as a circle with the center of *(-ψ', -χ')* and radius of *r'*. Capability curve of MMCs are plotted in Fig. 7. The smallest circles shown in Fig. 7(a) and Fig. 7(b) are typical MMC CC with $i_{dc}>0$ and $i_{dc}<0$ respectively.

By increasing the positive values of i_{dc} and decreasing the negative values of i_{dc}, CC can vary as depicted in Fig. 7 for different dc-link current values. As shown in these figures, the positive and negative areas of CC are significantly altered for both active and reactive power by changing dc-link currents. This has to be noted while designing any control process.

VII. DC-LINK VOLTAGE STABILITY ANALYSIS

How the changes of different variables available in the proposed HVDC system affect the dc-link voltage stability is discussed in this section.

With respect to (22), next equation can be inferred as,

$$C_{dc}\frac{dv_{dc}}{dt}+\frac{v_{dc}}{R_{dc}}=-\frac{P_1+P_2}{v_{dc}} \tag{28}$$

Applying small signal linearization to (28), the relation between dc link voltage and MMC active power variation is obtained as,

$$\left(C_{dc}s+\frac{1}{R_{dc}}-\frac{P_1^*+P_2^*}{v_{dc}^{*2}}\right)\Delta v_{dc}=-\frac{\Delta P_1+\Delta P_2}{v_{dc}^*} \tag{29}$$

By substituting (25) in (24), (30) is achieved as,

$$v_{dc}i_{dci}=P_i+\frac{L}{2}\frac{di_{di}^2}{dt}+Ri_{di}^2+\frac{L}{2}\frac{di_{qi}^2}{dt}+Ri_{qi}^2 \tag{30}$$

Another relation between Δv_{dc} and ΔP_i can be derived by the use of small signal linearization for (30) as,

$$\Delta P_i=\Delta v_{dc}i_{dci}^*+v_{dc}^*\Delta i_{dci}-\left(Ls+2R\right)i_{di}^*\Delta i_{di}-\left(Ls+2R\right)i_{qi}^*\Delta i_{qi} \tag{31}$$

By substituting (31) in (29), the effects of active power of MMC1 and MMC2 on the dc link voltage can be stated as (32) and (33) respectively,

$$\left[\Delta v_{dc}\middle|\left\langle\Delta P_2=0\right\rangle\right]=\left[\Delta v_{dc1}\right]=$$

$$\begin{bmatrix}\frac{(Ls+2R)i_{d1}^*}{\Delta_1} & \frac{(Ls+2R)i_{q1}^*}{\Delta_1} & -\frac{v_{dc}^*}{\Delta_1}\end{bmatrix}\begin{bmatrix}\Delta i_{d1}\\ \Delta i_{q1}\\ \Delta i_{dc1}\end{bmatrix}=\begin{bmatrix}f_{11} & f_{12} & f_{13}\end{bmatrix}\begin{bmatrix}\Delta i_{d1}\\ \Delta i_{q1}\\ \Delta i_{dc1}\end{bmatrix} \tag{32}$$

$$\left[\Delta v_{dc}\middle|\left\langle\Delta P_1=0\right\rangle\right]=\left[\Delta v_{dc2}\right]=$$

$$\begin{bmatrix}\frac{(Ls+2R)i_{d2}^*}{\Delta_2} & \frac{(Ls+2R)i_{q2}^*}{\Delta_2} & -\frac{v_{dc}^*}{\Delta_2}\end{bmatrix}\begin{bmatrix}\Delta i_{d2}\\ \Delta i_{q2}\\ \Delta i_{dc2}\end{bmatrix}=\begin{bmatrix}f_{21} & f_{22} & f_{23}\end{bmatrix}\begin{bmatrix}\Delta i_{d2}\\ \Delta i_{q2}\\ \Delta i_{dc2}\end{bmatrix} \tag{33}$$

Considering steady state operational condition of (28), Δ_i is equal to,

$$\Delta_i=\left(C_{dc}v_{dc}^*s+\frac{2v_{dc}^*}{R_{dc}}+i_{dci}^*\right) \tag{34}$$

Using (32) and (33), each part of dc-link voltage variations can be rewritten as follows,

$$\Delta v_{dci}=f_{i1}\Delta i_{di}+f_{i2}\Delta i_{qi}+f_{i3}\Delta i_{dci} \tag{35}$$

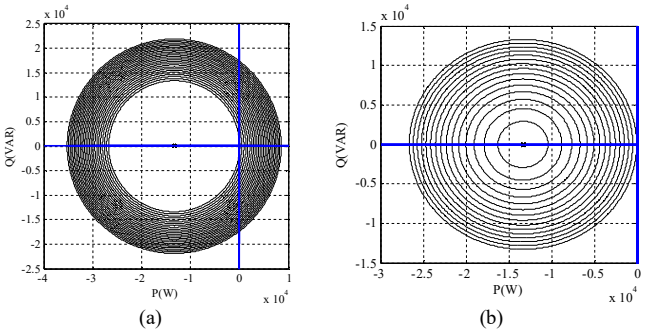

Fig. 7. Capability curve of MMCs (a) increasing $i_{dc}>0$, (b) decreasing $i_{dc}<0$.

Thus, the effects of the MMC d-q components and dc-link currents variation on dc-link voltage stability can be evaluated by (35). The Nyquist diagrams of each f_{ij} for various positive increasing values of dc-link current are separately depicted in Fig. 8. As realized from Fig. 8 (a) and Fig. 8 (b), f_{i1} and f_{i2} cannot lead to a noticeable instability in dc-link voltage. But, according to Fig. 8 (c), f_{i3} significantly increases the instability margins in both generation and control processes of dc-link voltage in HVDC system. For this case, regulating dc-link current at desired value is a vital operation in order to reach a stable dc-link voltage.

The same discussion is governed for various negative decreasing values of dc-link current as shown in Fig. 9. However, by decreasing the negative values of dc-link current, f_{i3} diagram is gone to the right-hand part and its magnitude is drastically decreased as illustrated in Fig. 9 (c) and consequently improves the stabilizing properties of f_{i3}.

VIII. SIMULATION RESULTS

The purpose of this section is to assess the capability of the proposed control scheme at reaching the desired values of MMC currents, voltages, and active and reactive power under both dynamic and steady state operating conditions. System parameters and the MMC rated values are listed in Table I.

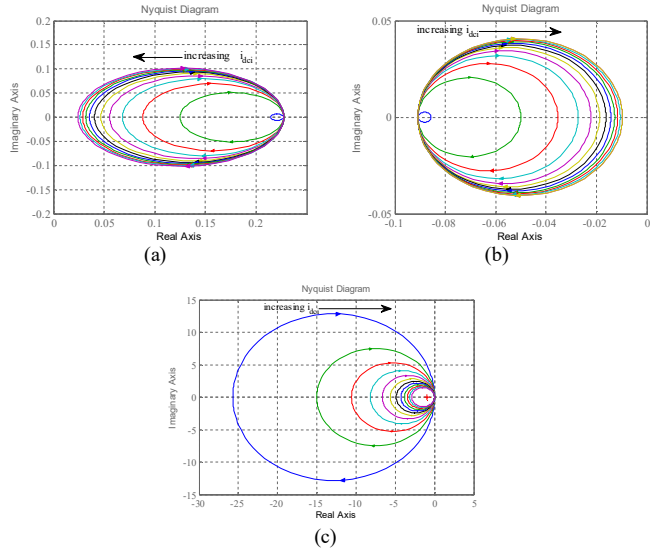

Fig. 8. Nyquist diagram of dc-link voltage variations for $i_{dci}>0$ due to (a) d-component variations of MMC current (f_{i1}) (b) q-component variations of MMC current (f_{i2}) (c) dc-link current variations (f_{i3}).

This article has been accepted for publication in a future issue of this journal, but has not been fully edited. Content may change prior to final publication. Citation information: DOI 10.1109/TPWRD.2016.2604295, IEEE Transactions on Power Delivery

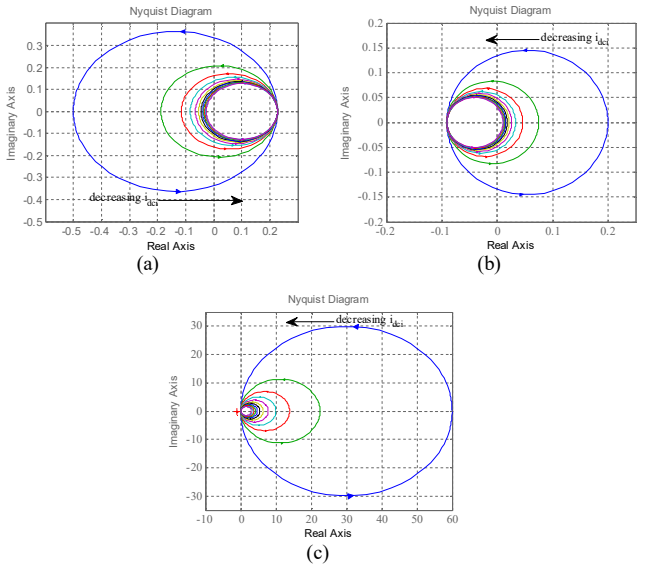

Fig.9. Nyquist diagram of dc-link voltage variations for $i_{dci}<0$ due to: (a) d-component variations of MMCs currents (f_{i1}), (b) q-component variations of MMCs currents (f_{i2}), and (c) dc-link current variations (f_{i3}).

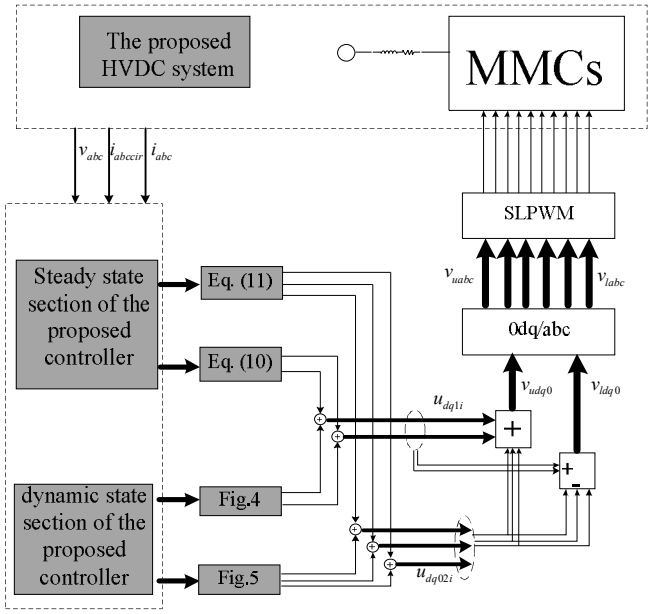

Fig.10. Overall structure of the proposed controller.

SimPower package of Matlab software is utilized to execute this assessment process as structured in Fig 10. For the modulation method, SLPWM technique is selected to synthesize gate switching signals for MMCs. To show effectively the impact of DLM on the stability of the proposed controller, two simulation processes will be considered. As a common operation in both processes, firstly the proposed HVDC system works in steady state and each MMC is responsible to supply active and reactive power required by the respective loads. Then, in the second time of each simulation, load changes take place at t=0.4s and t=0.6 s for MMC1 and MMC2, respectively, in which, in the first process DLM is not used, while the completed proposed controller with DLM is employed in the second process. The results are presented and discussed in the following section.

A. dc-link and ac voltages evaluation

Figs. 11 and 12 shows SM voltages and also dc and ac side voltages of MMCs in two simulation processes: without and with DLM. As can be observed, appropriate steady-state operation for dc-link voltage, upper and lower SMs voltages, and ac side voltages of MMCs are achieved with DLM.

TABLE I
UNITS FOR MAGNETIC PROPERTIES

f_{ac}	60 Hz	C	4mF
f_s	10 kHz	C_{fi}	650μF
v_{dc}^*	18kV	P_i	20MW
v_c	3kV	Q_i	10MVAR
L	45mH	Transformer power rating	8kV/23kV (Δ/Y)
R	0.3Ω	MMC1 load I	75MW,-25MVAR
L_t	12mH	MMC1 load II	85MW,80MVAR
R_t	1Ω	MMC2 load I	20MW,7MVAR
n	6	MMC2 load II	35MW,25MVAR

Fig. 11 shows that not using DLM in the proposed controller leads to the divergence of MMCs voltages from its desired values when the load changes happen for MMC1 and MMC2 at t=0.4s and t=0.6s, respectively.

Fig. 12 demonstrates the accurate operation of the proposed controller included DLM in both dynamic and steady states. According to this figure, in response to a transient variation, the dc link voltage is kept in desired value with small deviations.

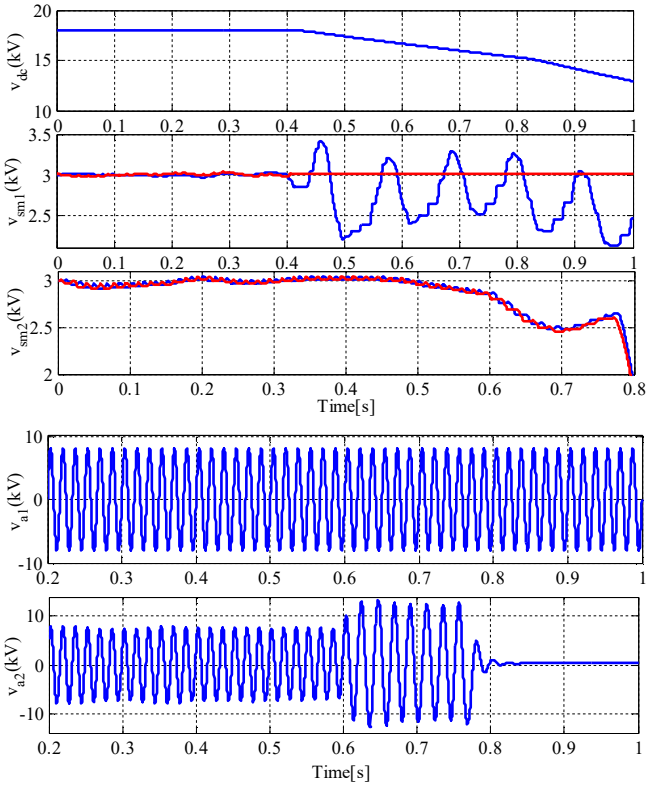

Fig.11. SM voltages and dc and ac side voltages of MMCs without DLM.

This article has been accepted for publication in a future issue of this journal, but has not been fully edited. Content may change prior to final publication. Citation information: DOI 10.1109/TPWRD.2016.2604295, IEEE Transactions on Power Delivery

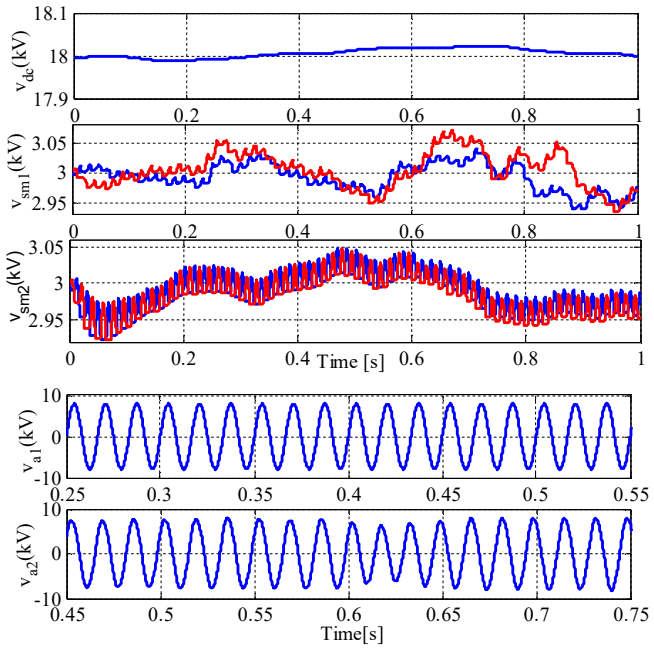

Fig.12. SM voltages and dc and ac side voltages of MMCs with DLM.

In addition, during both dynamic and steady operation of the proposed controller, the upper and lower SMs voltages follow the reference value of $v_{dc}^{*}/6$ with acceptable fluctuations.

The appropriate ac side voltages of MMCs are also obtained as shown in Fig. 12. The MMC2 should act as an inverter and consequently generation of sinusoidal and balanced ac voltages is a main duty of MMC2, which is completely performed as depicted in Fig. 12.

B. Analysis of MMC currents

To verify suitable performance of the proposed control technique for minimizing MMC circulating currents and regulating dc-link and ac currents of MMCs, Figs. 13 and 14 can be referred to.

Fig. 13 shows the simulation results of the proposed MMC-based HVDC system under operation of the proposed controller without DLM. As it can be understood from this figure, when load changes take place for MMCs, the controller without DLM is not able to keep the proposed system in stable operation and consequently the currents of MMC1 and MMC2 become unstable at t=0.4 s and t=0.6 s, respectively.

From circulating current waveforms of Fig. 14, it can be derived that minimizing these currents in both MMCs are properly done by the steady state section of the proposed controller and subsequently, in case of sudden loads changes, DLM fully provides dynamic control requirements in order to keep the currents at the minimized values.

Moreover, Fig. 14 shows the dc link currents of MMC1 and MMC2 respectively in both dynamic and steady states. Considering the dynamic step change time of t=0.4s and t=0.6s for MMC1 and MMC2 respectively, the duration of transient time and transient error values are insignificant in the second simulation process with DLM. Also the ac-side currents of MMCs are shown in Fig. 14.

As can be seen, current waveforms and their changes are proportional to the instantaneous needs of the load. They are also influenced by the function of keeping output voltages of MMC2 sinusoidal and balanced.

The d and q components of MMC currents are shown in Figs. 15 and 16. As can be seen, these components become unstable when DLM is not considered in the proposed control technique. When DLM is used in dynamic state operation of the proposed HVDC system, these currents move on their desired values with a small transient response time.

C. Active and reactive power sharing assessment

The proposed control technique of MMC is also responsible to provide the active and reactive power demanded from the proposed HVDC system.

MMCs active and reactive power waveforms are illustrated in Figs. 17 and 18. Firstly, MMC1 and MMC2 are aimed to supply loads of 10MW+j(-10)MVAR and 3MW+j0.7MVAR respectively. Then, another set of loads as 8MW+j9MVAR and 7MW+j4MVAR are connected to MMC1 and MMC2 respectively at t=0.4s and t=0.6s, respectively.

Fig. 17 verifies that the proposed controller without DLM cannot lead to a stable active and reactive power sharing for MMCs in dynamic operating condition.

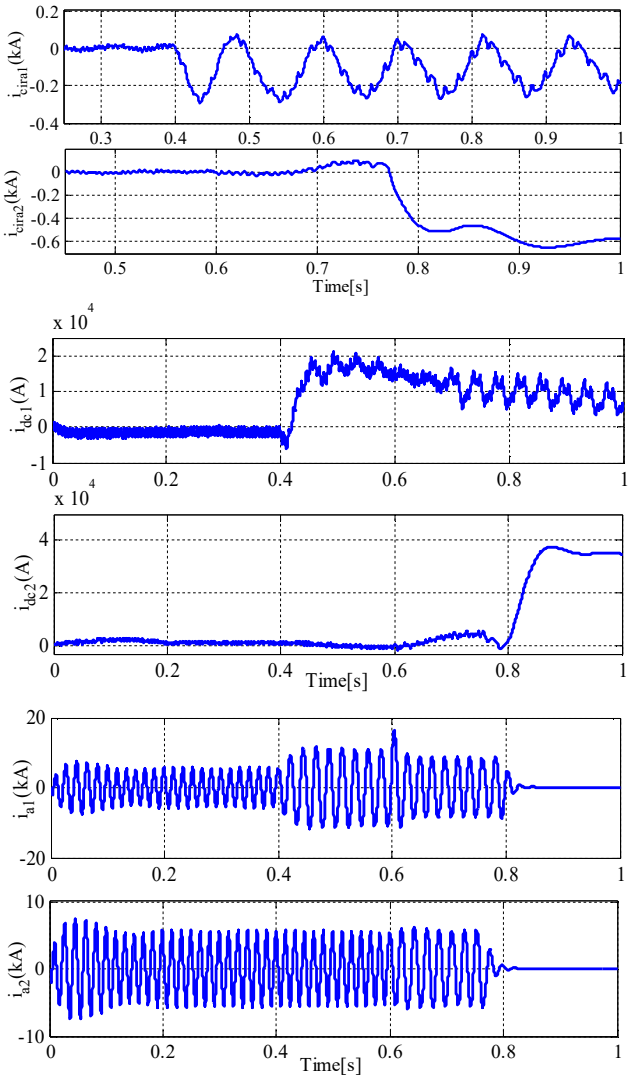

Fig. 13. Circulating, dc-link and ac-side currents of the interfaced MMCs without DLM.

This article has been accepted for publication in a future issue of this journal, but has not been fully edited. Content may change prior to final publication. Citation information: DOI 10.1109/TPWRD.2016.2604295, IEEE Transactions on Power Delivery

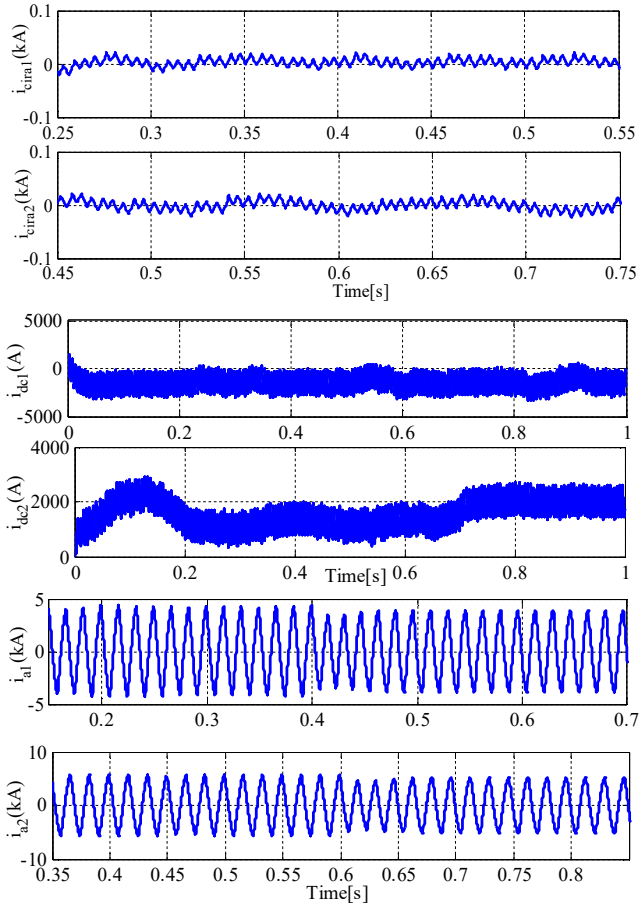

Fig. 14. Circulating, dc-link and ac-side currents of the interfaced MMCs with DLM.

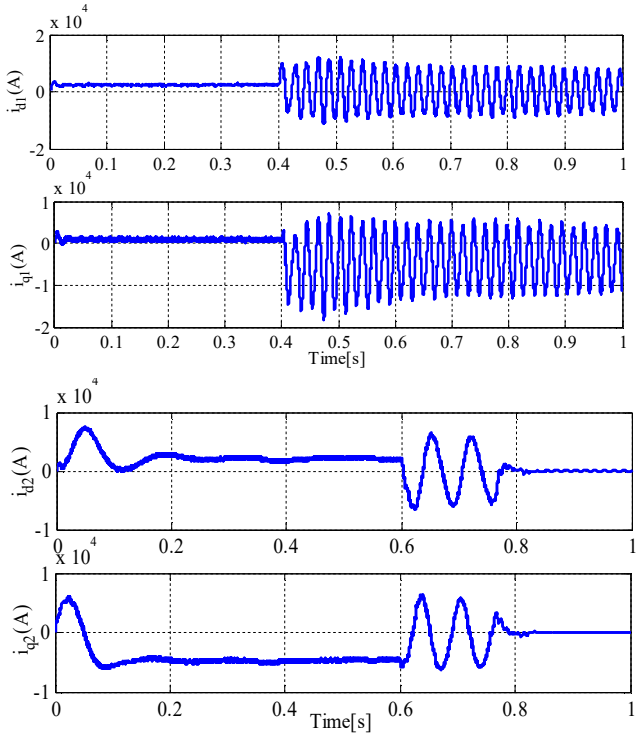

Fig. 15. d and q components of MMCs currents without DLM.

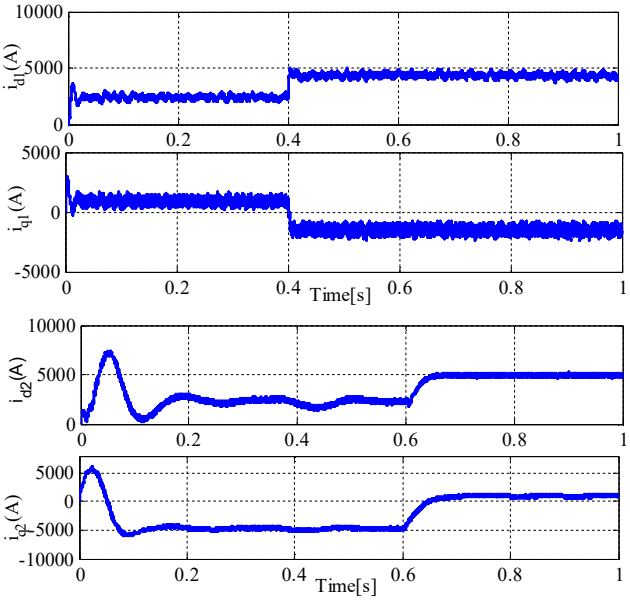

Fig. 16. d and q components of MMCs currents with DLM.

On the other hand, as can be seen in Fig. 18, MMCs active power orientation is in the direction of its respective load active power. Also the dynamic change of loads is highly compensated with a fast transient response, due to the proper controlled reaction operated by the designed DLM as depicted in Fig. 18.

Moreover, according to Fig. 18, the reactive power injection by MMC1 is due to the presence of respective reactive loads in both steady state and dynamic operating conditions of the proposed HVDC system, even though the scenario is different for MMC2. Fig. 18 also shows that due to presence of filter capacitance at the output of MMC2 for the aim of achieving the desired sinusoidal voltages, MMC2 consumes reactive power.

IX. Conclusion

This paper presented a d-q frame based model of MMC-HVDC with six independent dynamical state variables, including ac and circulating currents and also dc-link voltage, to effectively obtain the switching functions of MMC as well as for accurate circulating current control. Based on the reference values of selected state variables, the MMC switching functions under steady state were obtained to regulate the MMC operation in this state. Moreover, DLM was employed to develop dynamic parts of switching functions to reach globally asymptotically stability. In fact, using DLM leads to a proper operation of the designed controller and a better stabilization of MMC-HVDC against dynamic changes. Then, capability curve analysis of the interfaced MMCs in the proposed system was carried out by considering the effects of dc-link current changes. Furthermore, effects of MMC output and dc-link current variations on the dc-link voltage stability were evaluated in detail. Finally, the validity of the proposed controller for the proposed MMC-HVDC system was thoroughly verified and demonstrated by analyzing the simulation results achieved in Matlab/Simulink environment modeling.

This article has been accepted for publication in a future issue of this journal, but has not been fully edited. Content may change prior to final publication. Citation information: DOI 10.1109/TPWRD.2016.2604295, IEEE Transactions on Power Delivery

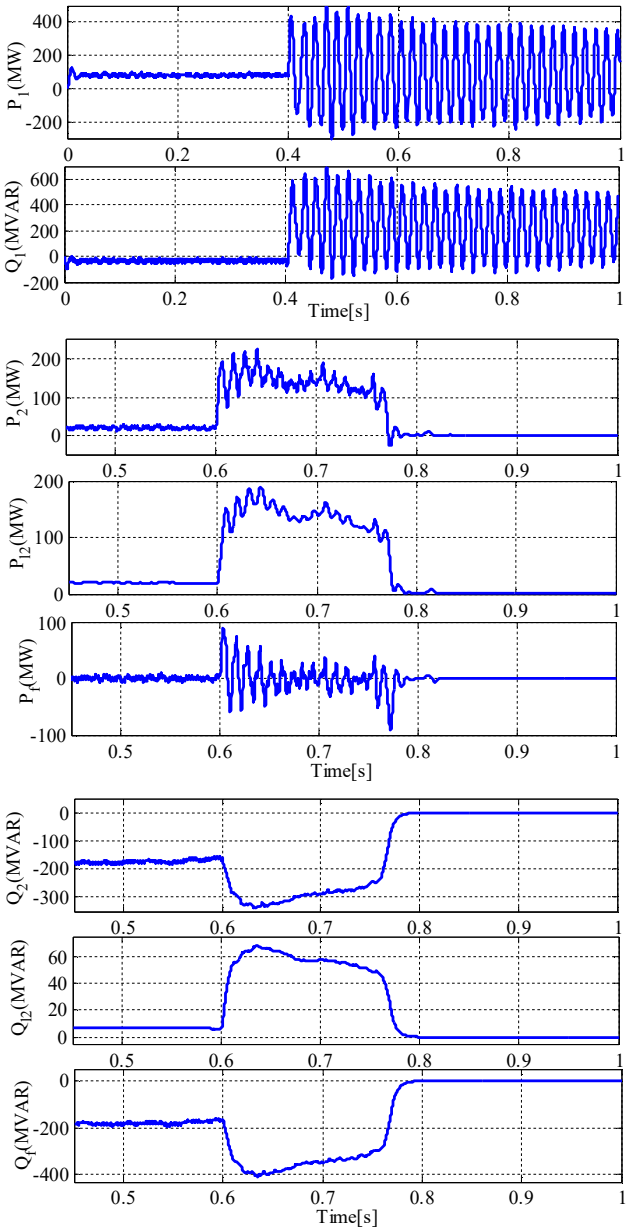

Fig.17. MMC1 and MMC2 active and reactive power waveforms without DLM.

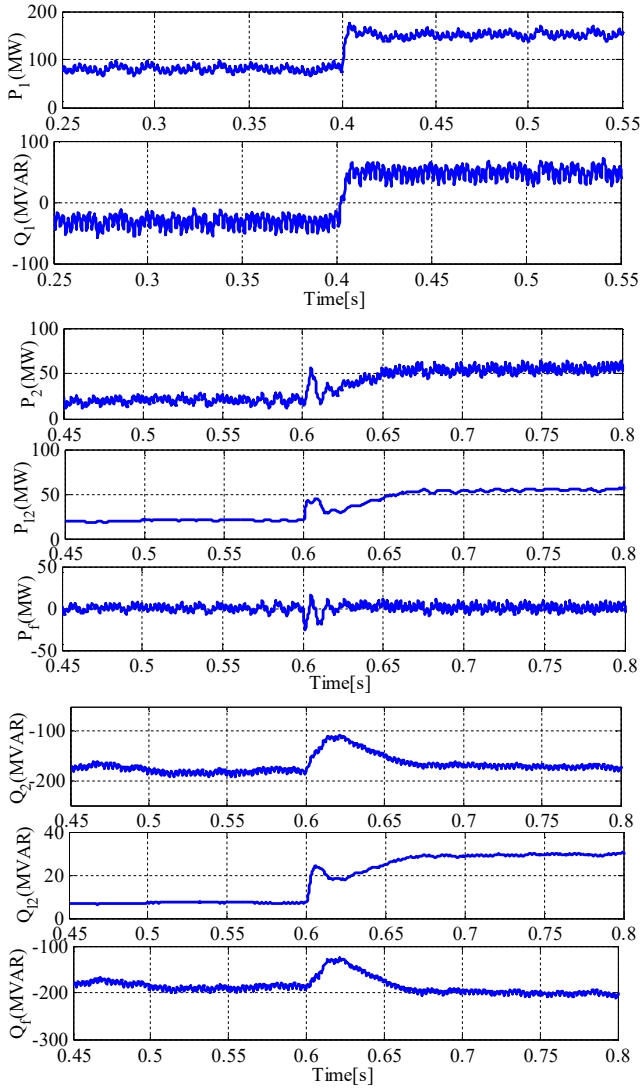

Fig.18. MMC1 and MMC2 active and reactive power waveforms with DLM.

REFERENCES

[1] H. Fehr, A. Gensior, and M. Muller, "Analysis and trajectory tracking control of a modular multilevel converter," *IEEE Trans. Power Electron*., vol. 30, no. 1, pp. 398-407, Jan. 2014.

[2] U. N. Gnanarathna, A.M. Gole, and R. P. Jayasinghe, "Efficient modeling of modular multilevel HVDC converters (MMC) on electromagnetic transient simulation programs," *IEEE Trans. Power Del*.,vol. 26, no. 1, pp. 316–324, Jan. 2011.

[3] M. Vatani, M. Hovd, M. Saeedifard, "Control of the Modular Multilevel Converter Based on a Discrete-Time Bilinear Model Using the Sum of Squares Decomposition Method," *IEEE Trans. Power Del*., vol. 30, no. 5, pp. 2179 - 2188, Oct. 2015.

[4] E. Pouresmaeil, M. Mehrasa, M. A. Shokridehaki, E. Rodrigues, and J. P. S. Catalao, "Control of Multi Modular Converters for Integration of Distributed Generation Sources into the Power Grid," in *Proc. IEEE International Conference on Smart Energy Grid Engineering (SEGE)*, pp. 1-6, Aug. 2015.

[5] S. Du, J. Liu, and T. Liu, "Modulation and Close-loop based DC Capacitor Voltage Control for MMC with Fundamental Switching Frequency," *IEEE Trans. Power Electron*., vol. 30, no. 1, pp. 327 - 338, Jan. 2015.

[6] H. Saad, J. Peralta, S. Dennetiere, J. Mahseredjian, J. Jatskevich, J.A, Martinez, A. Davoudi, M. Saeedifard, V. Sood, X. Wang, J. Cano, and A. Mehrizi-Sani, "Dynamic Averaged and Simplified Models for MMC-Based HVDC Transmission Systems," *IEEE Trans. Power Del*., vol. 28, no. 3, pp. 1723 - 1730, July. 2013.

[7] M. Saeedifard, and R. Iravani, "Dynamic Performance of a Modular Multilevel Back-to-Back HVDC System," *IEEE Trans. Power Del*., vol. 25, no. 4, pp. 2903 - 2912, Oct. 2010.

[8] A. Beddard, M. Barnes, and R. Preece, "Comparison of Detailed Modeling Techniques for MMC Employed on VSC-HVDC Schemes," *IEEE Trans. Power Del*., vol. 30, no. 2, pp. 579-589, April. 2015.

[9] L. Harnefors, A. Antonopoulos, S. Norrga, L. Angquist and H-P Nee, "Dynamic Analysis of Modular Multilevel Converters," *IEEE Trans. Industrial Elec.*, vol. 60, no. 7, pp. 2526 - 2537, July. 2013.

[10] P. Hu, and D. Jiang, "A Level-Increased Nearest Level Modulation Method for Modular Multilevel Converters," *IEEE Trans. Power Electron*., vol. 30, no. 4, pp. 1836 - 1842, April. 2015.

[11] B. Li, R. Yang, D. Xu, G. Wang, W. Wang, and D. Xu, "Analysis of the Phase-Shifted Carrier Modulation for Modular Multilevel Converters," *IEEE Trans. Power Electron*., vol. 30, no. 1, pp. 297 - 310, Jan. 2015.

[12] A. Dekka, B. Wu, and N.R Zargari, "A Novel Modulation Scheme and Voltage Balancing Algorithm for Modular Multilevel Converter," *IEEE Applied Power Electronics Conference and Exposition (APEC)*, pp. 1227-1233, March. 2015.

[13] W. Wang, A. Beddard, M. Barnes, and O. Marjanovic, "Analysis of Active Power Control for VSC–HVDC," *IEEE Trans. Power Del.*, vol. 29, no. 4, pp. 1978-1988, Aug. 2014.

[14] S. Liu, Z. Xu, W. Hua, G. Tang and Y. Xue, "Electromechanical Transient Modeling of Modular Multilevel Converter Based Multi-Terminal HVDC Systems," *IEEE Trans. Power System.*, vol. 29, no. 1, pp. 72 - 83, Jan. 2014.

[15] G. Bergna, E. Berne, P. Egrot, P. LefrancA. Arzandé, J.C Vannier, and M. Molinas, "An Energy-based Controller for HVDC Modular Multilevel Converter in Decoupled Double Synchronous Reference Frame for Voltage Oscillations Reduction," *IEEE Trans. Industrial Electron.*, vol. 60, no. 6, pp. 2360-2371, June. 2013.

[16] P. Wang, X. P. Zhang, P. F. Coventry, and R. Zhang, "Start-Up Control of an Offshore Integrated MMC Multi-Terminal HVDC System With Reduced DC Voltage," *IEEE Trans. Power System.*, vol. pp, no. 99, pp. 1 - 12, Sep. 2015.

[17] A. Antonopoulos, L. Ängquist, L. Harnefors, K. Ilves and H. P. Nee, "Global Asymptotic Stability of Modular Multilevel Converters," *IEEE Trans. Industrial Electron.*, Vol. 61, no. 2, pp. 603-612, Feb. 2014.

[18] S. Fan, K. Zhang, J. Xiong, and Y. Xue, "An Improved Control System for Modular Multilevel Converters with New Modulation Strategy and Voltage Balancing Control," *IEEE Trans. Power Electron.*, vol. 29, no. 9, pp. 4568-4579, Sep. 2014.

[19] M. Zhang, L. Huang, W. Yao, and Z. Lu, "Circulating Harmonic Current Elimination of a CPS-PWM Based Modular Multilevel Converter with Plug-In Repetitive Controller," *IEEE Trans. Power Electron.*, vol. 29, no. 4, pp. 2083 - 2097, April. 2014.

[20] J.-W. Moon, J.-S. Gwon, J.-W. Park, D.-W. Kang, and J.-M. Kim, "Model Predictive Control With a Reduced Number of Considered States in a Modular Multilevel Converter for HVDC System," *IEEE Trans. Power Del.*, vol. 30, no. 2, pp. 608 - 617, April. 2015.

[21] M.A. Perez, S. Bernet, J. Rodriguez, S. Kouro, and R. Lizana, "Circuit Topologies, Modelling, Control Schemes and Applications of Modular Multilevel Converters," *IEEE Trans. Power Electron.*, vol. 30, no. 1, pp. 4-17, Jan. 2015.

[22] J. Wang, R. Burgos, and D. Boroyevich, "Switching-Cycle State-Space Modeling and Control of the Modular Multilevel Converter," *IEEE Journal of Emerging and Selected Topics in Power Electronics*, vol. 2, no. 4, pp. 1159 - 1170, Dec. 2014.

[23] F. Yu, W. Lin, X. Wang, and D. Xie, "Fast Voltage-Balancing Control and Fast Numerical Simulation Model for the Modular Multilevel Converter," *IEEE Trans. Power Del.*, vol. 30, no. 1, pp. 220 - 228, Feb. 2015.

[24] Y. Li, E. A. Jones, and F. Wang, "The Impact of Voltage-Balancing Control on Switching Frequency of the Modular Multilevel Converter," *IEEE Trans. Power Electron.*, vol. 31, no. 4, pp. 2829 - 2839, April 2016.

[25] R. Lizana, M.A Perez, S. Bernet, J.R Espinoza, and J. Rodriguez, "Control of Arm Capacitor Voltages in Modular Multilevel Converters," *IEEE Trans. Power Electron.*, vol. 31, no. 2, pp. 1774 - 1784, Feb 2016.

[26] R. Lizana, M.A Perez, D. Arancibia, J.R Espinoza, and J. Rodriguez, "Decoupled Currents Model and Control of Modular Multilevel Converters," *IEEE Trans. Industrial Electron.*, vol. 62, no. 9, pp. 5382 - 5392, Sep 2015.

[27] M. Mehrasa, E. Pouresmaeil, M.F. Akorede, B.N Jørgensen, and J.P.S Catalao, "Multilevel Converter Control Approach of Active Power Filter for Harmonics Elimination in Electric Grids," *Energy.*, vol. 84, pp. 722 - 731, May 2015.

Majid Mehrasa received the B.Sc. and M.Sc. degrees in electrical engineering from the University of Mazandaran, Babol, Iran, in 2006 and 2009, respectively.

He is currently with the Young Researchers and Elite Club, Sari Branch, Islamic Azad University, Sari, Iran. His current research interests include power electronic applications to power system and the use of nonlinear control theories for various power converters.

Edris Pouresmaeil (M'14) received the B.Sc. and M.Sc. degrees in Electrical Engineering from the University of Mazandaran, Babol, Iran, in 2003 and 2005, respectively. He received the Ph.D. degree in Electrical Engineering with honor from the Technical University of Catalonia. Barcelona Tech. (UPC), Barcelona, Spain, in 2012.

After his Ph.D. he joined the Department of Electrical & Computer Engineering, at the University of Waterloo, Canada, as a Postdoctoral Research Fellow, and later he joined the Department of Electromechanical Engineering, at the University of Beira Interior, Portugal. He was an Associate Professor in Energy Technology Engineering at the University of Southern Denmark (SDU), Denmark, and Senior Researcher at Abengoa Research, Spain. He is currently a Senior Researcher with the Institute Super Tecn Lisbon (INESC-ID), Portugal.

His research interests include application and control of power converters in intelligent power systems, stability analysis of power converters in power system, and integration of large-scale renewable energy sources into the low-inertia power grid.

Sasan Zabihi received the B.Sc. (Eng.) and M.Sc. (Eng.) degrees in Electrical Engineering–Telecommunication and Power respectively in 2003 and 2006 from Technical Universities in Iran. After 2 years in industry and academia, he started a Ph.D. program in Power-Electronics at Queensland University of Technology (QUT), Brisbane, Australia. He completed his PhD in 2011, and from 2011 to 2012, he was a lecturer with QUT. Since 2013 he is working as R&D design specialist for ABB/Australia in CoC for MicroGrid, renewable integration, and distributed generation.

His research interests include power-electronics topologies, control and applications, pulsed power, MicroGrid, renewable energy integration, and distributed generation.

João P. S. Catalão (M'04-SM'12) received the M.Sc. degree from the Instituto Superior Técnico (IST), Lisbon, Portugal, in 2003, and the Ph.D. degree and Habilitation for Full Professor ("Agregação") from the University of Beira Interior (UBI), Covilha, Portugal, in 2007 and 2013, respectively.

Currently, he is a Professor at the Faculty of Engineering of the University of Porto (FEUP), Porto, Portugal, and Researcher at INESC TEC, INESC-ID/IST-UL, and C-MAST/UBI. He was the Primary Coordinator of the EU-funded FP7 project SiNGULAR ("Smart and Sustainable Insular Electricity Grids Under Large-Scale Renewable Integration"), a 5.2-million-euro project involving 11 industry partners. He has authored or coauthored more than 475 publications, including 157 journal papers, 281 conference proceedings papers, 23 book chapters, and 14 technical reports, with an *h*-index of 27 and over 3000 citations (according to Google Scholar), having supervised more than 45 post-docs, Ph.D. and M.Sc. students. He is the Editor of the books entitled *Electric Power Systems: Advanced Forecasting Techniques and Optimal Generation Scheduling* and *Smart and Sustainable Power Systems: Operations, Planning and Economics of Insular Electricity Grids* (Boca Raton, FL, USA: CRC Press, 2012 and 2015, respectively). His research interests include power system operations and planning, hydro and thermal scheduling, wind and price forecasting, distributed renewable generation, demand response and smart grids.

Prof. Catalão is an Editor of the IEEE TRANSACTIONS ON SMART GRID, an Editor of the IEEE TRANSACTIONS ON SUSTAINABLE ENERGY, and an Associate Editor of the *IET Renewable Power Generation*. He was the Guest Editor-in-Chief for the Special Section on "Real-Time Demand Response" of the IEEE TRANSACTIONS ON SMART GRID, published in December 2012, and the Guest Editor-in-Chief for the Special Section on "Reserve and Flexibility for Handling Variability and Uncertainty of Renewable Generation" of the IEEE TRANSACTIONS ON SUSTAINABLE ENERGY, published in April 2016. He was the recipient of the 2011 Scientific Merit Award UBI-FE/Santander Universities and the 2012 Scientific Award UTL/Santander Totta. Also, he has won 4 Best Paper Awards at IEEE Conferences.